Hyperfine Coupling Constants of the Azafullerenes $C_{19}N$, $C_{59}N$, $C_{69}N$, and $C_{75}N$†

Joshua Schrier*

Computational Research Division, Lawrence Berkeley National Laboratory, Berkeley, California 94720

K. Birgitta Whaley

Department of Chemistry and Pitzer Center for Theoretical Chemistry, University of California, Berkeley, California 94720

Received: November 8, 2005; In Final Form: February 9, 2006

The isomers of the nitrogen-substituted fullerenes (azafullerenes) $C_{19}N$, $C_{59}N$, $C_{69}N$, and $C_{75}N$ are examined using all-electron Gaussian atomic orbital basis density functional theory, to determine the doublet radical geometries and hyperfine coupling constants. We find that the inaccuracy of previously calculated hyperfine coupling constants of $C_{59}N$ resulted from a poor treatment of the geometry optimization. We find that UB3LYP minimization of the radical geometry in the 6-31G* basis, followed by single-point evaluation of the hyperfine constants in which an expanded basis is used on the atomic sites of interest, forms an efficient compromise between computational cost and accuracy with respect to experimental hyperfine constants. Using this approach, we assign the hyperfine signals observed in experiments on the $C_{69}N$ radical by calculating the hyperfine coupling constants for all five of the isomers and examine the electron spin density distribution. Finally, we present predicted hyperfine coupling constants for the isomers of $C_{19}N$ and $C_{75}N$ for use in the interpretation of future experiments.

I. Introduction

Following the early theoretical predictions of the stability of $C_{59}N$,[1] and subsequent synthesis and isolation,[2] the study of fullerenes in which one or more of the carbon atoms are substituted by a nitrogen atom (azafullerenes) has attracted much attention (reviewed by Hirsch and Nuber[3]). Besides fundamental interest, modification of the chemical and electrical properties of parent fullerenes has led to several practical applications. Recent experiments using single $C_{59}N$ azafullerene molecules in double-barrier tunnel junctions have demonstrated single electron tunneling and electrical rectification.[4] Additionally, the electron-donating azafullerenes may be added in arbitrary amounts (unlike stoichiometrically fixed alkali fulleride compounds), to dope the semiconductive (1.5 eV band gap[5]) C_{60} solid. To this end, solid solutions of $C_{59}N$ in C_{60} have been prepared,[6] and ESR experiments indicate that the unpaired electrons are bound to the $C_{59}N$ species.[7] This offers a possible architecture for solid-state quantum computation, utilizing the (hyperfine coupling mediated) electron−nuclear spin entanglement schemes demonstrated in crystalline malonic acid[8] and substitutional nitrogen vacancies (N−V defects) in diamond.[9] The use of azafullerenes offers the advantage that the electron spin properties may be systematically tuned by varying the size, shape, and substitutional site of the parent fullerene molecule.

Both $C_{59}N$[6,7,10,11] and $C_{69}N$[12] have been studied by electron spin resonance (ESR) spectroscopy, to determine the properties of the free radical electron of these molecules. However, the theoretical study of the hyperfine coupling constants (hfccs) of these molecules has not been pursued as extensively. Early calculations by Fülöp et al. of the hfccs of $C_{59}N$, using a PM3-optimized geometry followed by single-point UB3LYP/6-31G* calculations of the doublet radical, yielded highly inaccurate results.[6] Subsequently, Csányi and Arias presented a planewave pseudopotential local spin density (LSDA) method, using a projector-augmented wave (PAW) formalism, that more accurately reproduced the experimental values for the ^{13}C and ^{14}N hfccs of $C_{59}N$[13] and has subsequently been applied to the study of $C_{59}N$-doped C_{60} solids.[7]

Recent benchmarking studies by Hermosilla et al. have found that geometry optimization of radicals is important in obtaining accurate hfccs when using atomic orbital-basis density functional calculations.[14,15] Their results suggest that a reason for the failure of the earlier all-electron atomic orbital DFT calculations may have been a relatively poor treatment of radical geometries by semiempirical methods, which is magnified by the sensitivity of the hfcc. Based on their small molecule results, Hermosilla et al. suggest that, for large radicals, UB3LYP/6-31G* should give qualitatively accurate results, provided that the geometry optimization of the radical is performed at the same level. Additionally, their latter work found larger basis sets to give relatively small changes to the geometry, suggesting that geometric optimization with 6-31G*, followed by a single-point calculation of the hfccs with a larger basis set should perform adequately.[15] The hfcc is strongly dependent on the ability of the basis set to describe the nuclear region, a task at which Gaussian basis sets typically perform poorly. However, the relatively economical 6-31G* basis reasonably describes the overall geometry and spin density distribution. Therefore, use of the TZVP or EPR-III at the atomic sites of interest, which are designed for a better description of the nuclear region, should improve the local description of the hfcc without increasing the basis size in the remainder of the molecule. We examine this suggestion here as it applies to the azafullerenes $C_{19}N$, $C_{59}N$, $C_{69}N$, and $C_{75}N$. In the cases of $C_{59}N$ and $C_{69}N$, comparison is made to existing experimental and theoretical results; the

† Part of the special issue "John C. Light Festschrift".

10.1021/jp056462m CCC: $33.50
Published on Web 03/14/2006

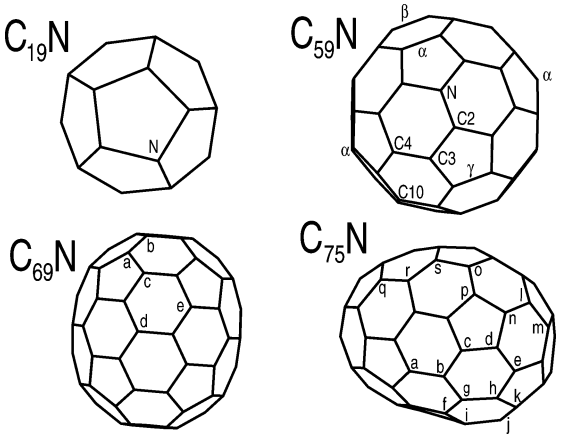

Figure 1. Site labeling scheme for the azafullerene isomers studied in this work. The $C_{19}N$ and $C_{59}N$ azafullerenes each have only one symmetry-unique nitrogen substitution site. Labels for $C_{59}N$ follow the scheme used in refs 6 and 13, with carbon atoms labeled by roman characters and C−C bonds of interest by greek characters. The lowercase roman labels for $C_{69}N$ and $C_{75}N$ indicate the unique substitutional isomers derived from the parent fullerenes.

remaining cases serve as predictions. We expect the hfcc results to be of use in the interpretation of current and future ESR data, and the optimized radical geometries to be a starting point for future theoretical studies.

II. Computational Method

The 6-31G, 6-31G*, TZVP,[16] and EPR-III[17] basis sets were utilized in this study, together with the unrestricted B3LYP[18,19] density functional. Previous calculations of vacancy defect fullerenes by Hu and Ruckenstein found the B3LYP/6-31G* method to agree with experimental bond lengths.[20,21] All density functional calculations were performed with revisions B.04 and C.02 of the Gaussian 03 package,[22] and the PM3[23] calculations were performed using Mopac2002.[24] The starting geometry for the $C_{19}N$, $C_{59}N$, $C_{69}N$, and $C_{75}N$ azafullerenes were based on the I_h, I_h, D_{5h}, and D_2 symmetry parent carbon fullerenes, respectively,[25] with nitrogen atoms substituted into the symmetry unique sites as shown in Figure 1.

For all of the 6-31G and 6-31G* cases, we performed a full energy minimization of the particular structure. The small size of the $C_{19}N$ azafullerene allowed us to perform a full energy minimization using the TZVP (EPR-III) basis on every atom. For the other molecules, the 6-31G* optimized doublet radical geometry was used to perform a single-point calculation using the TZVP (EPR-III) basis on only the nitrogen atom and, in the case of $C_{59}N$, also on four surrounding carbon atoms. All other atoms in these cases were treated with the 6-31G* basis. We also examined geometry relaxation in these mixed basis calculations for the $C_{59}N$ molecule, indicated as TZVP† and EPR-III† in Table 2.

The isotropic hyperfine coupling constant for nucleus K is given by[26]

$$a_K = \frac{\mu_0}{3} g_e \mu_B g_K \mu_K \langle S_z \rangle^{-1} \rho_K \qquad (1)$$

where μ_0 is the vacuum permeability, g_e and g_K are the electron and nuclear g factors, μ_B and μ_K are the Bohr and nuclear magnetons, and $\langle S_z \rangle$ the expectation value of the Pauli S_z operator for the given electronic state. The Fermi contact integral for nucleus K is given by

$$\rho_K = \sum_{\mu\nu} \langle \phi_\mu(\vec{r}) | \delta(\vec{r} - \vec{r}_K) | \phi_\nu(\vec{r}) \rangle P_{\mu\nu}^{spin} \qquad (2)$$

where $\phi_\mu(\vec{r})$ are the basis functions and δ is the Dirac delta function acting on the integrated position variable $\vec{r}$ and the nuclear position $\vec{r}_K$. The one-electron spin density matrix, $P_{\mu\nu}^{spin} = (P_{\mu\nu}^{\alpha} - P_{\mu\nu}^{\beta})$ is the difference between the spin α and β one-electron density matrixes, constructed by summing over the α-spin occupied states

$$P_{\mu\nu}^{\alpha} = \sum_{i \in occ(\alpha)} c_{\mu i}^{\alpha} (c_{\nu i}^{\alpha})^* \qquad (3)$$

using the coefficients of the spin-unrestricted wave functions

$$\psi_i^{\alpha} = \sum_{\mu} c_{\mu i}^{\alpha} \phi_\mu(\vec{r}) \qquad (4)$$

III. Results and Discussion

The results for the ^{14}N hfccs are shown in Tables 1−4; the corresponding optimized geometries are given in the Supporting Information. We first examine the $C_{19}N$ azafullerene (Table 1). Because of its relatively small size, which allowed for full geometry optimization calculations with large basis sets, this highly strained molecule should serve as a rigorous test for the possible basis set convergence in the description of the hfcc, as was suggested by the studies of Hermosilla et al.[14,15] As shown in Table 1, we find that the 6-31G*, TZVP, and EPR-III basis sets give qualitatively similar results for the ^{14}N hfcc. In contrast, the 6-31G basis set result differs substantially from these for $C_{19}N$.

The results for $C_{59}N$ are shown in Table 2; since both experimental and theoretical results for the ^{13}C hfccs are available for this species, we will discuss these in more detail. In the experiment, typically only the magnitude of the hfccs may be determined; all of the theoretical calculations agree in the assignment of a negative sign to the $^{13}C_3$ hfcc. In general, we find that the 6-31G* based hfcc values match experiments better than the PM3//UB3LYP/6-31G* values calculated by Fülöp et al.[6] but not as well as the PAW results of Csányi and Arias.[13] As shown in Table 2, we find that use of the mixed basis approach generally brings the calculated hfcc into closer agreement with the experimental values than the 6-31G* results. Only the ^{14}N hfcc is shifted away from the experimental value by a few percent; in the case of the C_3, C_4, and C_{10} hfccs, the results obtained in this manner are comparable to those of the PAW method. We also note that comparable results are obtained for both the TZVP and EPR-III cases, despite a 11% smaller basis for the former, which leads to a substantial reduction in computational time. Furthermore, relaxation of $C_{59}N$ with either the mixed TZVP/6-31G* or EPR-III/6-31G* basis sets yields hfcc results of comparable accuracy (as judged by the root-mean-square error with respect to the experiments) to the more expensive PAW method. This is primarily due to the improved C_2 hfcc, which is closer to experiment than the PAW result, although we note that this is accompanied by a slight reduction in the agreement of the C_4 hfcc. Although this improved average agreement is pleasing, this approach of mixed-basis minimiza-

TABLE 1: Calculated ^{14}N hfccs (in Gauss) for $C_{19}N$[a]

	6-31G	6-31G*	TZVP	EPR-III
$C_{19}N$	1.47	4.18	4.13	4.33

[a] The columns indicate the basis set used on all of the atoms for both the geometry optimization and hfcc evaluation.

TABLE 2: Comparison of ^{14}N and ^{13}C hfccs (in mT, 1 mT = 0.1 G) for $C_{59}N$[a]

atom	6-31G	6-31G*	TZVP	EPR-III	TZVP†	EPR-III†	expt.[6]	PAW[13]	PM3[6]
N	0.45	0.42	0.42	0.44	0.41	0.40	0.36	0.33	0.87
C_2	2.51	1.93	1.51	1.52	1.30	1.33	1.18	1.38	2.29
C_3	−0.88	−0.65	−0.65	−0.60	−0.64	−0.61	0.48	−0.40	−0.80
C_4	0.96	0.68	0.48	0.49	0.46	0.46	0.52	0.55	0.88
C_{10}	0.56	0.39	0.26	0.26	0.26	0.26	0.25	0.30	0.44
rms	0.59	0.34	0.17	0.16	0.10	0.10		0.10	0.50

[a] The labeling of the sites is shown in Figure 1. Experimental values and the PM3-based geometry calculations (followed by UB3LYP/6-31G* determination of the hfccs) are from Fülöp[6] The projector-augmented wave (PAW) results are from Csányi and Arias.[13] As described in the text, the TZVP and EPR-III results were obtained by performing a single point calculation on the 6-31G* optimized geometry, with the addition of the TZVP or EPR-III basis set on the atomic sites the specific sites listed above. The TZVP† and EPR-III† results were obtained by adding the specified basis to the specific atomic sites, and then allowing a geometry relaxation of the structure, followed by hfcc evaluation in that basis. The root-mean-square (rms) error of the calculated results, with respect to the experimental values, is listed in the final row.

TABLE 3: Comparison of ^{14}N Hyperfine Coupling Constants (in Gauss) for $C_{69}N$ to the Experimental Values of Hasharoni[12a]

	6-31G*	TZVP	EPR-III	signal	expt.[12]
$C_{69}N$-a	3.82	3.65	3.49		
$C_{69}N$-b	5.19	5.01	4.91	A	4.74
$C_{69}N$-c	2.78	2.47	2.52		
$C_{69}N$-d	−0.58	−0.57	−0.41	B	0.49
$C_{69}N$-e	2.65	2.48	2.72		

[a] The site labeling scheme is depicted in Figure 1. As described in the text, the TZVP (EPR-III) results are obtained by first optimizing the doublet radical geometry in the 6-31G* basis, followed by single-point calculation of the hfcc using the TZVP (EPR−III) basis on the nitrogen atom. Our assignment matches that of Hasharoni for the origin of signal A, but differs in the assignment of signal B.

TABLE 4: Calculated ^{14}N hfccs (in Gauss) for $C_{75}N$[a]

	6-31G*	TZVP	EPR-III
$C_{75}N$-a	1.69	1.52	1.57
$C_{75}N$-b	−0.08	−0.15	0.36
$C_{75}N$-c	1.99	1.77	1.71
$C_{75}N$-d	1.88	1.71	1.65
$C_{75}N$-e	3.14	2.93	2.73
$C_{75}N$-f	0.97	0.72	0.73
$C_{75}N$-g	1.37	1.23	1.19
$C_{75}N$-h	2.56	2.32	2.31
$C_{75}N$-i	1.64	1.45	1.45
$C_{75}N$-j	0.60	0.43	0.43
$C_{75}N$-k	1.45	1.14	0.45
$C_{75}N$-l	4.48	4.33	3.97
$C_{75}N$-m	5.12	5.04	4.80
$C_{75}N$-n	4.27	4.13	3.77
$C_{75}N$-o	1.91	1.67	1.68
$C_{75}N$-p	2.67	2.35	2.36
$C_{75}N$-q	1.73	1.62	1.70
$C_{75}N$-r	0.11	0.17	0.35
$C_{75}N$-s	0.71	0.48	0.49

[a] The labeling schemes for the isomers are depicted in Figure 1. The 6-31G* column indicates that both the geometry optimization and hfcc evaluation were performed in this basis; the TZVP (EPR-III) column shows values obtained using the 6-31G* optimized geometry, followed by a single point evaluation of the hfcc using the TZVP (EPR-III) basis on the nitrogen atom. All calculations were performed on the doublet radical species.

tion may however not be fully justified, since it breaks some of the symmetry of the problem.

In Figure 2, we compare the $C_{59}N$ bond lengths determined by the PM3 and UB3LYP/6-31G* geometry optimizations. The largest differences between the bond lengths calculated by the two methods are 0.05 Å for the two N−C bonds along the pentagon−hexagon (6:5) edges and 0.03 Å for hexagon−hexagon (6:6) edge. The five largest C−C bond length differences are indicated by the greek-labeled bonds in Figure 1. In particular, the three α labeled bonds differ by 0.021 Å, the β bond differs by 0.019 Å, and the δ bond by 0.018 Å. We also observe that the C−C 6:5 bonds in the PM3 structure are systematically longer than the density functional results. Despite the deformation of the fullerene cage being primarily near the impurity site,[1] the errors in the PM3 geometry affect the more distant bonds as well. We suspect that this results from the lack of an explicit doublet-radical parametrization for the PM3 method.

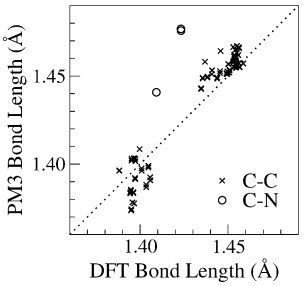

Figure 2. Comparison of the optimized $C_{59}N$ bond-lengths determined by PM3 versus the present UB3LYP/6-31G* density functional approach. The dotted line indicates the bisectrix.

We next examine the five symmetry-unique sites for the nitrogen atom in the $C_{69}N$ azafullerene. Table 3 shows the ^{14}N hfcc values and compares these to the corresponding experimental measurements of Hasharoni et al.[12] In the experiment, only two different signals were observed, which the authors labeled "A" and "B", respectively. Since our calculated ^{14}N hfcc values for the various isomers differ by more than a Gauss from each other, we may unambiguously assign signals A and B to the $C_{69}N$-b and $C_{69}N$-d isomers, respectively. As noted above, only the magnitudes of the hfcc are determined by these experiments, so the negative sign does not detract from this agreement. Comparing to the assignments depicted in Figure 2 of the paper by Hasharoni et al.,[12] we agree with their assignment for the isomer giving rise to signal A but differ in the assignment of that giving rise to signal B. Use of the TZVP and EPR-III basis sets on the nitrogen atoms somewhat improves the quantitative agreement with experiment. The ^{14}N hfcc values are plotted together with the corresponding (6-31G*-basis calculated) ^{13}C hfcc values in Figure 3.

In addition to calculating the ^{14}N and ^{13}C hfcc values, we also evaluated the electron spin density distribution for the two isomers $C_{69}N$-b and $C_{69}N$-d that were assigned above to the experimentally observed signals. In Figure 4, we have plotted the spin density distribution of these two species, as determined from the 6-31G* basis calculations. The largest contributions to the spin density in the $C_{69}N$-b isomer are localized on the nitrogen atom and on the nearby carbon atoms. In contrast, the spin density of the $C_{69}N$-d isomer is distributed over the hemisphere containing the nitrogen atom. Two of the nearest-

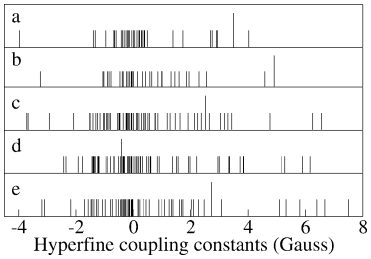

Figure 3. ^{14}N (tall lines) and ^{13}C (short lines) hfccs for the five $C_{69}N$ isomers, in Gauss. The labels a−e denote the sites defined in Figure 1. Only the $C_{69}N$-b and $C_{69}N$-d isomers are near the observed ^{14}N values of magnitude 4.74 and 0.49 G.[12]

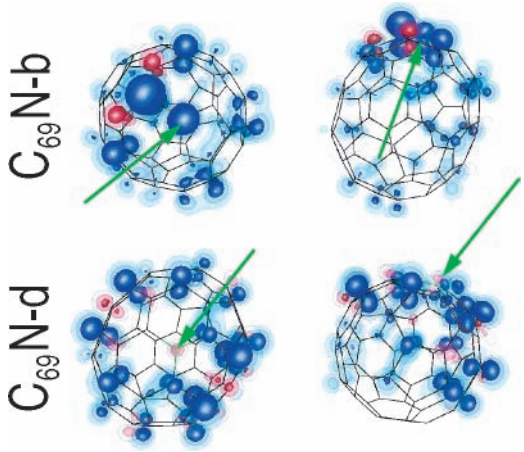

Figure 4. Spin density isocontour plots for the $C_{69}N$-b and $C_{69}N$-d isomers. The green arrows point to the nitrogen atom position in each structure. In the $C_{69}N$-b isomer, the nitrogen atom is hidden below the second-largest positive (blue) contour in the center of the top view. The positive spin density is shown as blue, and the negative spin density is shown in red.

neighbor carbons to the nitrogen have positive spin density, but the largest contributions to the positive spin density are on two of the next-nearest-neighbor carbons. There is also a particularly large-magnitude negative spin density centered on the carbon atoms third-nearest-neighbor to the nitrogen atom. Since the hfcc is proportional to the spin density at the nucleus, we also note that the localization of the spin density may be used to select where to increase the basis size when performing larger-basis calculations of the ^{13}C hfccs.

Finally, we discuss the ^{14}N hfccs of the 19 isomers of the $C_{75}N$ azafullerene, shown in Table 4. No previous experimental or theoretical calculations of the hfcc properties of these molecules are available, so we confine our analysis here to a few general remarks. First, the $C_{75}N$ ^{14}N hfcc values span a large range of magnitude, suggesting that their identities should be readily assignable experimentally. Second, we note that with the exception of the b and r isomers of $C_{75}N$, using the EPR-III basis on the nitrogen defect center reduces the magnitude of the ^{14}N hfcc value, as compared to the value obtained with the 6-31G* basis. Most dramatically, $C_{75}N$-k shows a reduction of 1 G in magnitude. In these anomalous cases, the TZVP results are in better agreement with the 6-31G* values than the EPR-III results. Since none of the previous calculations described in the current study encountered a similar case of qualitative disagreement between the TZVP and EPR-III hfcc values, further geometry optimization with larger basis functions may be desirable before attributing future experimental results to these particular species. Otherwise, the TZVP values are intermediate to, or in agreement with, the EPR-III values, with the hfccs in the larger basis showing a typical reduction by 0.2−0.3 G, as compared to the 6-31G* values, similar to the effects observed in Table 2 for $C_{59}N$ and in Table 3 for the $C_{69}N$ isomers.

IV. Conclusion

We have determined the geometries and isotropic hfcc of the azafullerenes $C_{19}N$, $C_{59}N$, $C_{69}N$, and $C_{75}N$. Our results agree with previous experimental and planewave pseudopotential results for $C_{59}N$ and are used to assign the origin of the signals in $C_{69}N$ observed in experiment. Additionally, our results support the conclusion of Hermosilla et al.[14,15] that use of large basis sets for geometry optimization of radicals is necessary to obtain accurate hfccs using density functional methods. In future studies comparing the performance of atom-centered orbital and planewave methods, it will be useful to identify the relative contributions of effects deriving from basis set completeness of the electron-wave function near the nucleus, versus effects of geometry. Should the near-nuclear description play the more important role, nuclear-cusp constraint methods, such as proposed by Galek et al.,[27] may be useful in improving the quality of atomic-orbital basis results. Finally, we note that recent density functional calculations for the interpretation of EPR experiments on C_{60} bisadduct anions have relied on the PM3-based geometries;[28] significant improvement may be achieved using the approach we describe above.

Acknowledgment. J.S. thanks Dr. Lin-Wang Wang for a careful reading of the manuscript. This work was supported by the U. S. Department of Energy under Contract No. DE-AC03-76SF00098, the Defense Advanced Research Projects Agency (DARPA) and the Office of Naval Research under Grant No. FDN00014-01-1-0826, and the National Science Foundation under Grant EIA-0205641.

Supporting Information Available: Corresponding optimized geometries. This material is available free of charge via the Internet at http://pubs.acs.org.

References and Notes

(1) Andreoni, W.; Gygi, F.; Parrinello, M. *Chem. Phys. Lett.* **1992**, *190*, 159.
(2) Hummelen, J. C.; Knight, B.; Pavlovich, J.; Gonzalez, R.; Wudl, F. *Science* **1995**, *269*, 1554.
(3) Hirsch, A.; Nuber, B. *Acc. Chem. Res.* **1999**, *32*, 795.
(4) Zhao, J.; Zeng, C.; Cheng, X.; Wang, K.; Wang, G.; Yang, J.; Hou, J. G.; Zhu, Q. *Phys. Rev. Lett.* **2005**, *95*, 045502.
(5) Oshiyama, A.; Saito, S.; Hamada, N.; Miyamoto, Y. *J. Phys. Chem. Solids* **1992**, *53*, 1457.
(6) Fülöp, F.; Rockenbauer, A.; Simon, F.; Pekker, S.; Korecz, L.; Garaj, S.; Jánossy, A. *Chem. Phys. Lett.* **2001**, *334*, 233.
(7) Rockenbauer, A.; Csányi, G.; Fülöp, F.; Garaj, S.; Korecz, L.; Lukács, R.; Simon, F.; Forró, L.; Pekker, S.; Jánossy, A. *Phys. Rev. Lett.* **2005**, *94*, 066603.
(8) Mehring, M.; Mende, J.; Scherer, W. *Phys. Rev. Lett.* **2003**, *90*, 153001.
(9) Popa, I.; Gaebel, T.; Domhan, M.; Wittmann, C.; Jelezko, F.; Wrachtrup, J. *Phys. Rev. B* **2004**, *70*, 201203.
(10) Simon, F.; Arčon, D.; Tagmtarchis, N.; Garaj, S.; Forro, L.; Prassides, K. *J. Phys. Chem. A* **1999**, *103*, 6969.
(11) Simon, F.; Fülöp, F.; Rockenbauer, A.; Korecz, L.; Kuzmany, H. *Chem. Phys. Lett.* **2005**, *404*, 85.
(12) Hasharoni, K.; Bellavia-Lund, C.; Keshvarz-K., M.; Srdanov, G.; Wudl, F. *J. Am. Chem. Soc.* **1997**, *119*, 11128.
(13) Csányi, G.; Arias, T. A. *Chem. Phys. Lett.* **2002**, *360*, 552.
(14) Hermosilla, L.; Calle, P.; de la Vega, J. M. G.; Sieiro, C. *J. Phys. Chem. A* **2005**, *109*, 1114.
(15) Hermosilla, L.; Calle, P.; de la Vega, J. M. G.; Sieiro, C. *J. Phys. Chem. A* **2005**, *109*, 7626.
(16) Schäfer, A.; Huber, C.; Ahlrichs, R. *J. Chem. Phys.* **1994**, *100*, 5829.

(17) Barone, V. In *Recent Advances in Density Functional Methods*; Chong, D. P., Ed.; World Scientific: Singapore, 1996; Vol. 1.
(18) Becke, A. D. *J. Chem. Phys.* **1993**, *98*, 5648.
(19) Lee, C.; Yang, W.; Parr, R. G. *Phys. Rev. B* **1988**, *37*, 785.
(20) Hu, Y. H.; Ruckenstein, E. *J. Chem. Phys.* **2003**, *119*, 10073.
(21) Hu, Y. H.; Ruckenstein, E. *J. Chem. Phys.* **2004**, *120*, 7971.
(22) Frisch, M. J.; Trucks, G. W.; Schlegel, H. B.; Scuseria, G. E.; Robb, M. A.; Cheeseman, J. R.; Montgomery, J. A., Jr.; Vreven, T.; Kudin, K. N.; Burant, J. C.; Millam, J. M.; Iyengar, S. S.; Tomasi, J.; Barone, V.; Mennucci, B.; Cossi, M.; Scalmani, G.; Rega, N.; Petersson, G. A.; Nakatsuji, H.; Hada, M.; Ehara, M.; Toyota, K.; Fukuda, R.; Hasegawa, J.; Ishida, M.; Nakajima, T.; Honda, Y.; Kitao, O.; Nakai, H.; Klene, M.; Li, X.; Knox, J. E.; Hratchian, H. P.; Cross, J. B.; Adamo, C.; Jaramillo, J.; Gomperts, R.; Stratmann, R. E.; Yazyev, O.; Austin, A. J.; Cammi, R.; Pomelli, C.; Ochterski, J. W.; Ayala, P. Y.; Morokuma, K.; Voth, G. A.; Salvador, P.; Dannenberg, J. J.; Zakrzewski, V. G.; Dapprich, S.; Daniels, A. D.; Strain, M. C.; Farkas, O.; Malick, D. K.; Rabuck, A. D.; Raghavachari, K.; Foresman, J. B.; Ortiz, J. V.; Cui, Q.; Baboul, A. G.; Clifford, S.; Cioslowski, J.; Stefanov, B. B.; Liu, G.; Liashenko, A.; Piskorz, P.; Komaromi, I.; Martin, R. L.; Fox, D. J.; Keith, T.; Al-Laham, M. A.; Peng, C. Y.; Nanayakkara, A.; Challacombe, M.; Gill, P. M. W.; Johnson, B.; Chen, W.; Wong, M. W.; Gonzalez, C.; Pople, J. A. *Gaussian 03*; Gaussian Inc.: Wallingford, CT, 2004.
(23) Stewart, J. J. P. *J. Comput. Chem.* **1989**, *10*, 209.
(24) Stewart, J. J. P. *MOPAC 2002*, version 2.10; Fujitsu Limited: Tokyo, Japan, 2002.
(25) Fowler, P. W.; Manolopoulos, D. E. *An Atlas of Fullerenes*; Clarendon: Oxford, 1995.
(26) Sadlej, J. *Semiempirical Methods of Quantum Chemistry*; Wiley: New York, 1985.
(27) Galek, P. T.; Handy, N. C.; Cohen, A. J.; Chan, G. K.-L. *Chem. Phys. Lett.* **2005**, *404*, 156.
(28) Zoleo, A.; Bellinazzi, M.; Prato, M.; Brustolon, M.; Maniero, A. L. *Chem. Phys. Lett.* **2005**, *412*, 470.